ROCKET OZONESONDE (ROCOZ)—DESIGN AND DEVELOPMENT

by

A. J. Krueger
and
W. R. McBride

Research Department

ABSTRACT. This report describes the theory and design of an optical ozonesonde system developed for use on Arcas rockets. The payload is an ultraviolet filter photometer useful in the altitude range 20 to 60 km. A real-time digital data logging system has been constructed for recording the data that are telemetered on the 1680 mHz meteorological frequency. Data-processing procedures are described and results of a test flight are presented.

NAVAL WEAPONS CENTER
CHINA LAKE, CALIFORNIA • JULY 1968

NAVAL WEAPONS CENTER
AN ACTIVITY OF THE NAVAL MATERIAL COMMAND

M. R. Etheridge, Capt., USN ..... Commander
Thomas S. Amlie, Ph.D. ..... Technical Director

FOREWORD

This report describes the design, development, and testing of a system for measurement of the distribution of atmospheric ozone using meteorological rockets.

The objective of this program was to produce a light, compact, rugged, and inexpensive ozonesonde (ROCOZ) for use with Arcas rockets to collect data in the region from 20 to 60 km. Such an instrument was required to determine if ozone is in photochemical equilibrium with oxygen and ultraviolet sunlight as the present theory predicts.

This work is part of a program directed to the measurement of physical characteristics and composition of the stratosphere to an altitude of 60 km. The work complements the intensive balloon investigations of lower stratospheric ozone and bears a direct relationship to the Meteorological Rocket Network measurements of air temperature and winds.

Operational flights have been conducted at geographical locations of interest and results will be reported ir future publications.

The project was initially supported by the Office of Naval Research under Project Number NR 082-183 and then by the Pacific Missile Range Project Orders PO-3-0021/072831005 and PO-4-0005/073146202. Rockets and parachutes were furnished by the Geophysics Division of PMR.

Released by
P. ST.-AMAND, Head
Earth and Planetary Sciences Division
3 June 1968

Under authority of
HUGH W. HUNTER, Head
Research Department

NWC Technical Publication 4512

Published by.....Research Department
Collation.....Cover, 21 leaves, DD Form 1473, abstract cards
First printing.....150 unnumbered copies
Security classification.....UNCLASSIFIED

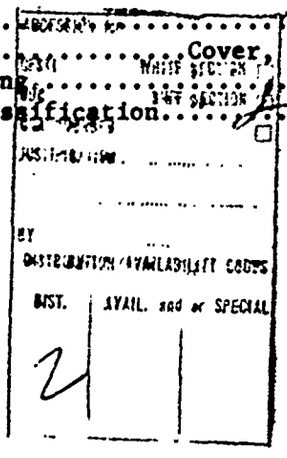

CONTENTS

ACKNOWLEDGMENT

The effort described herein has been possible only through the assistance of many people at this Center. Wm. L. Burson of the Research Department has contributed significantly in all phases of the project. Much of the original electronic design was accomplished under the direction of James P. Lee aided by Larry Pace and Douglas W. Cowan, all of the Weapons Development Department. H. P. Tempel, formerly with Associated Aero Science Laboratories, Inc., Ridgecrest, California, with Wm. L. Burson are responsible for the design evolution to a serviceable instrument for field operations and also were of primary assistance in conducting field operations. Vernon O. Jones of the Research Department contributed to the mechanical design, and Eugene J. Dibble also of the Research Department assembled and calibrated the optical components. Roy L. Zuber, formerly of the Systems Development Department, designed and constructed the digital data recording system. Wm. W. Baer and Donald Cooper, both of the Systems Development Department, provided electronic design assistance. Computer programming was done by Barbara A. Gonder, John B. Garber, and Gary Stevenson, all of the Systems Development Department.

INTRODUCTION

The rocket ozonesonde (ROCOZ), Fig. 1, developed at this Center is an optical instrument using the sun as a light source and four selected pass bands in the ultraviolet region from 2700 to 3300 Å to measure attenuation of solar energy by ozone. An Arcas rocket carries the ROCOZ to an altitude of 55 to 65 km and a gas generator ejects the payload for deployment on a parachute. The relatively slow rate of descent allows a longer time for measurement than would be obtained in free fall.

ROCOZ is designed as a sequential sampling filter photometer that makes use of a standard meteorological frequency and ground station for telemetry. An automatic digital recording system was constructed to receive the data on the ground.

The basic system operated successfully in test flights. However, the tests did show that the payload-parachute system must be stabilized to acquire higher quality analog data from this payload configuration over the entire altitude range.

THEORETICAL CONSIDERATIONS

OPTICAL TECHNIQUE FOR ATMOSPHERIC OZONE MEASUREMENTS

Ozone is characterized by an intense optical absorption band in the near ultraviolet. As measured by Inn and Tanaka (Ref. 1), the exponential absorption coefficient reaches a peak value of 311 cm^{-1} (base e) at 2553 Å, but decreases to less than 1 cm^{-1} for wavelengths greater than 3180 Å. With a typical total ozone amount of 0.3 cm n.t.p., essentially no radiation reaches the earth's surface at wavelengths less than 2950 Å. The total ozone amount in a column through the atmosphere is measured routinely at more than 100 stations around the world with the Dobson spectrophotometer and similar instruments by optical absorption at wavelengths longer than 3050 Å. These instruments compare the irradiance from extraterrestrial sources (primarily the sun) at wavelength pairs separated by approximately 200 Å.

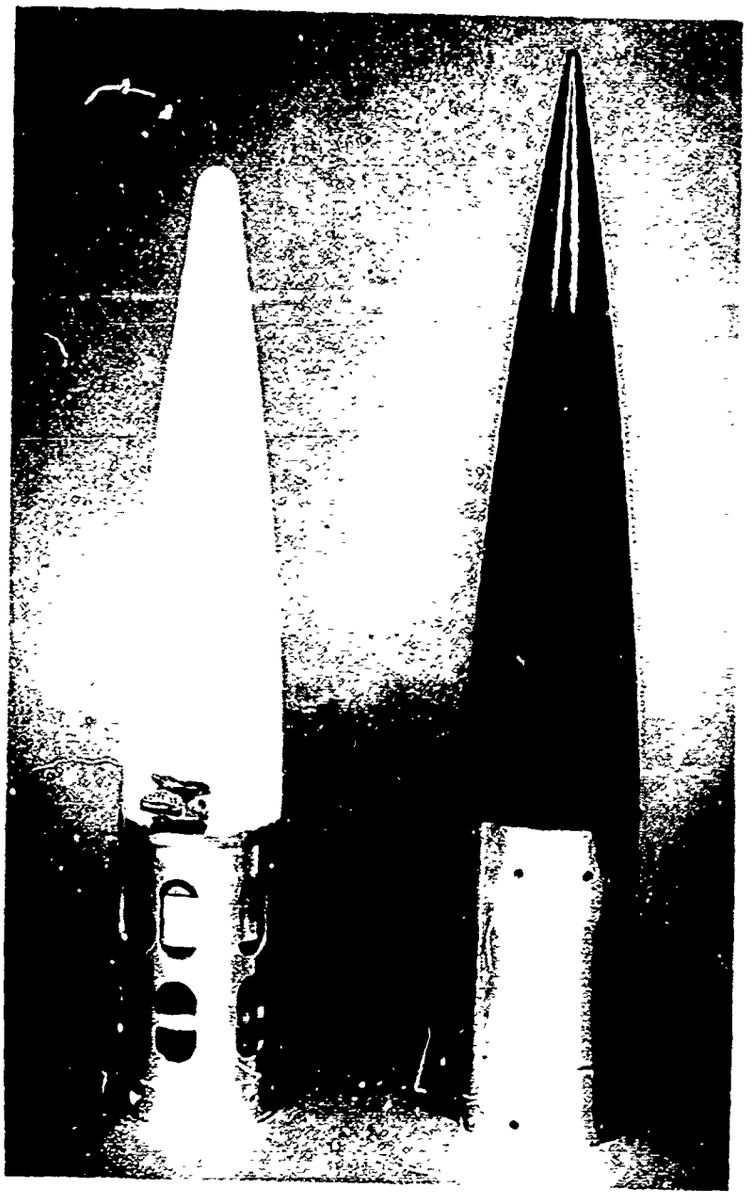

FIG. 1. Rocket Ozonesonde.

A similar approach has been used to determine the height distribution of ozone with balloon-borne spectrographs and photometers. Paetzold in Germany, Vassy in France, and Kobayashi, et al., in Japan have made numerous soundings with filter photometers (Ref. 2-4). The Paetzold instrument is equipped to telemeter data on solar irradiance in two spectral bands between 3000 and 4000 Å to ground stations. One band is located in the ozone absorption region; the other band where absorption is zero. The ozone concentration as a function of height is calculated from the change in irradiance in the absorbed band with height. To avoid having to point the optical axis these instruments are constructed with a wide field of view. This results in a moderation of the irradiance gradient at altitudes where the skylight is a significant component of the total irradiance. This is generally the case below 15-20 km, depending on the separation between the bands. The problem is, of course, most difficult at the ground where the Dobson spectrophotometer is used. Here both Rayleigh and Mie scattering provide large contributions to the skylight. Only by restricting the field of view and comparing overlapping wavelength pairs is the problem minimized.

From 20 km to normal maximum balloon altitudes the optical ozonesondes are capable of accurate measurement of the broad details of the ozone distribution. The ability to determine detailed structure is related to the accuracy of the height gradient of irradiance. With typical photometer and telemetry noise levels, data over at least 1 km are required to establish the gradient, and the resolution is typically 1 to 2 km, which for most research purposes is adequate.

SELECTION OF WAVELENGTHS FOR HIGH ALTITUDE MEASUREMENTS

In the balloon altitude regime, x(h), the total ozone remaining above height, h, ranges from a normal maximum of 0.5 cm at the ground to 0.1 cm at 30 km. The solar irradiance, $I(\lambda,h)$, at wavelength, λ, and height, h, depends on the absorption coefficient $\alpha(\lambda)$ and x(h), according to Beer's law:

$$I(\lambda,h) = I(\lambda,\infty) \exp[-\alpha(\lambda)\, x(h) \sec z] \qquad (1)$$

where z is the solar zenith distance and $I(\lambda,\infty)$ is the extraterrestrial solar irradiance. For low values of z, the relative irradiance at 3100 Å varies from 0.25 at the ground to 0.75 at 30 km. Above the primary ozone peak at 25 km the concentration is predicted by photochemical theory to decrease approximately exponentially with height. Early measurements on rockets using spectrographic payloads have indicated that this is correct. Whereas a single filter at 3100 Å (and a reference at a longer wavelength) has been adequate for balloon ozonesondes, this is no longer the case at higher altitudes where x(h) is expected to decrease by three orders of magnitude between 30 and 60 km.

If it is assumed that the ozone concentration, $\epsilon(h)$, above the primary peak can be represented by the function

$$\epsilon(h) = \epsilon_o \exp[-(h - h_o)/H]$$

where H is the ozone scale height, then the total ozone (above height h) is given by

$$x(h) = \epsilon_o H \exp[-(h - h_o)/H] \qquad (2)$$

The ozone concentration is determined from the change in irradiance with height. From Eq. 1 and 2, the following can be written for any wavelength

$$\frac{\partial I}{\partial h} = \alpha \epsilon_o I \sec z \exp[-(h - h_o)/H]$$

This function has a maximum at $h_m = h_o + H \ln H \alpha \epsilon_o \sec z$.

If h_m is selected as the reference height, it is found that

$$\frac{\partial I}{\partial h} \frac{H}{I_o} = \exp[-u - \exp(-u)]$$

where $u = (h - h_m)/H$. This function, shown in Fig. 2, was originally derived by Chapman, Ref. 5, to show that optical absorption in a plane exponential atmosphere takes place in relatively thin strata when the absorption coefficient is constant. In the present context, the maximum useful height range for a narrow-band optical filter can be determined from this curve. For example, assuming a scale height of 6 km and a minimum detectable change in irradiance of 2%/km, $\partial I/\partial h\ H/I_o = 0.12$. The absorption rate function exceeds this value between $u = -1.24$ and +1.98. This corresponds to a total height range of 19.3 km. These assumptions are not unrealistic and it can be expected that the irradiance at two wavelengths corresponding to different values of h_m will be required for ozone determinations over the altitude range from 30 to 60 km where the concentration decays exponentially with height. The optimum values of h_m are in the vicinity of 33 and 47 km. The wavelengths required to obtain these optimum heights can be calculated given the $\alpha(\lambda)$ curve and an estimate of x(h) sec z from the condition: $\alpha(\lambda)\ x(h_m) \sec z = 1$.

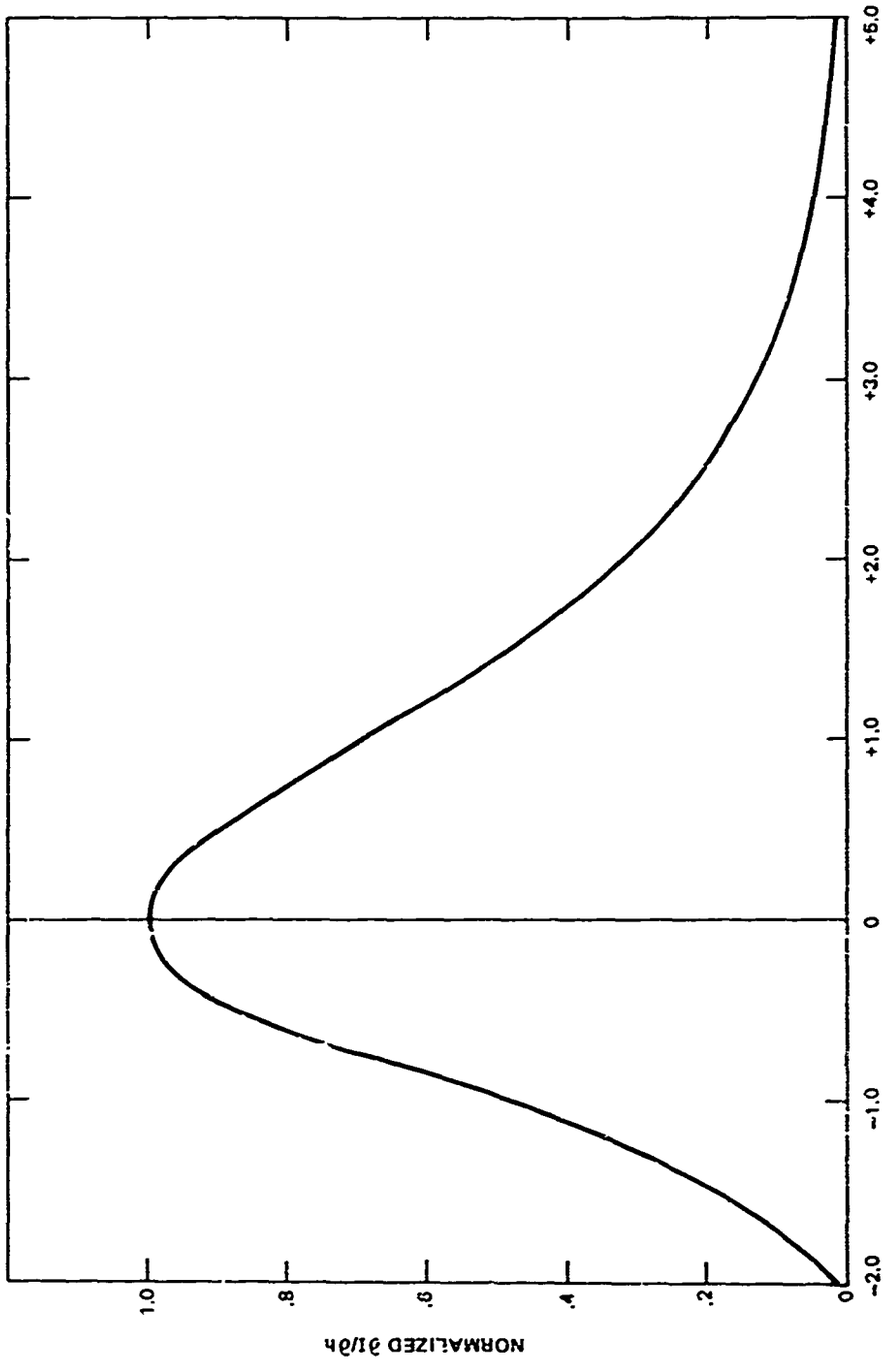

FIG. 2. Normalized ∂I/∂h vs. u.

Assuming a nominal z of 45 degrees

$$\alpha(\lambda_1) = 1/x(33 \text{ km}) \sec 45^\circ = 1/.05 \times 1.414 = 14.1 \text{ cm}^{-1}$$

$$\alpha(\lambda_2) = 1/x(47 \text{ km}) \sec 45^\circ = 1/.003 \times 1.414 = 238 \text{ cm}^{-1}$$

Following recommendations of Inn and Tanaka (Ref. 1), their measurements of $\alpha(\lambda)$ have been adopted for wavelengths less than 2750 Å and the measurements of Vigroux (Ref. 6) have been adopted for longer wavelengths because of the higher resolution. The absorption coefficients derived above correspond to center wavelengths of 2970 Å at 33 km and 2675 Å at 47 km. While these are optimum wavelengths some adjustment is made from consideration of the solar spectrum and the actual height range attainable with the Arcas system.

For the region below 30 km a band near 3100 Å is suitable as used in the Paetzold balloon sonde. For a reference filter where $\alpha(\lambda) = 0$ a center wavelength near 3300 Å has been adopted.

CALCULATION OF OZONE CONCENTRATIONS FROM THE OBSERVED IRRADIANCE DATA

In the calculation of the ozone distribution from irradiance data, Beer's law (Eq. 1) is used. However, the optical filters have bandwidths wide enough that the wavelength dependence of various input parameters must be recognized. It is possible to treat the ozone absorption coefficient and Rayleigh extinction coefficient as functions of the total ozone amount, x, and the relative air mass, m, because these are the parameters that result in an alteration of the spectrum as a function of height. An "effective absorption coefficient" is defined by:

$$\alpha_j(x,m) = -\frac{1}{x} \ln \left\{ \frac{\int_{\lambda_1}^{\lambda_2} I(\lambda,\infty)\, F_j(\lambda)\, P(\lambda)\, \tau(\lambda)\, \exp[-\alpha(\lambda)\, x - \beta(\lambda) m]\, d\lambda}{\int_{\lambda_1}^{\lambda_2} I(\lambda,\infty)\, F_j(\lambda)\, P(\lambda)\, \tau(\lambda)\, \exp[-\beta(\lambda) m]\, d\lambda} \right\} \quad (3)$$

where

$F_j(\lambda)$ = transmission function of the j^{th} filter
$\tau(\lambda)$ = transmission function of the integrating sphere
$P(\lambda)$ = photodetector response
$\beta(\lambda)$ = Rayleigh extinction coefficient

and the wavelength limits, λ_1 and λ_2, cover the wavelength region of interest. Because of variations between filters constructed for the various payloads, it has been necessary to calculate α_j for each new filter. Typical results are shown in Fig. 3.

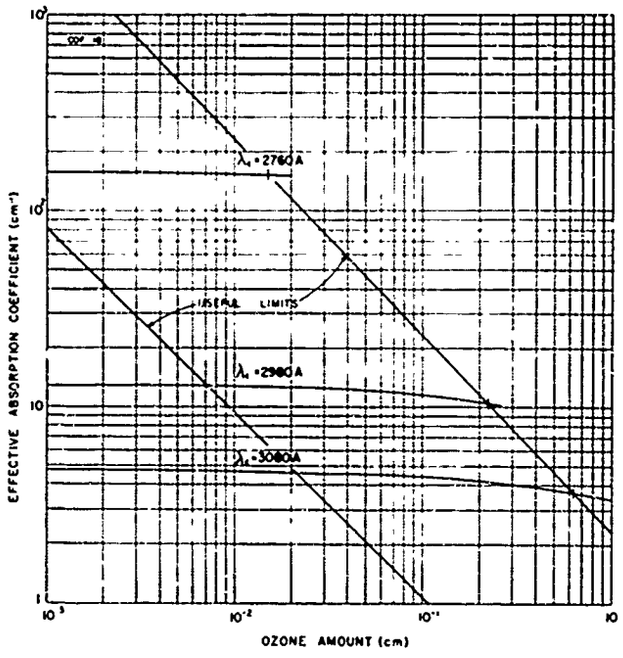

FIG. 3. Absorption Coefficients of Filters.

The basic absorption equation can then be written as the ratio of the output signals, $S_j(h)$, for the j^{th} filter and the reference filter ($j = o$).

$$\frac{S_j(h)}{S_o(h)} = \frac{S_j(\infty)}{S_o(\infty)} \exp\left\{-[\alpha_j(x,m) - \alpha_o(x,m)]\, x(h) \sec z\right\} \times \exp\left\{-[\beta_j(x,m) - \beta_o(x,m)]\, m(h)\right\} \tag{4}$$

where $\beta_j(x,m)$ is defined similarly to $\alpha_j(x,m)$. The extraterrestrial ratio ($h = \infty$) can be measured on a rocket flight in that the value of $\alpha_j x \approx 0$ at the top of the flight. At low altitudes ($h < 20$ km) skylight begins to contribute to the total irradiance as observed by Paetzold (Ref. 2). In the present analysis where the interest is primarily in the ozone concentrations in and above the primary peak this contribution can be ignored for the present time. As data are accumulated with the filters selected for this instrument, attempts will be made to derive corrections for application to the lower altitude data.

The ozone concentrations, $\Delta x(h)/\Delta h$, are calculated using a simplified form of a finite difference equation as derived by Paetzold (Ref. 2):

$$\frac{\Delta x(h)}{\Delta h}(\alpha_j - \alpha_o)\sec z = \frac{\Delta \ln S_j(h)/S_o(h)}{\Delta h} + \frac{\Delta d(h,z)}{\Delta h}\frac{\partial \alpha_j}{\partial d(h)}d(h,z) + \frac{\Delta \sec z}{\Delta h}\alpha_j x(h) + \frac{\Delta m(h,z)}{\Delta h}\Delta\beta_j + \frac{\Delta m(h,z)}{\Delta h}\frac{\partial \alpha_j}{\partial m(h,z)}m \quad (5)$$

where $d = x(h)\sec z$. This equation yields a solution by iteration given an assumed starting distribution, $d_1(h,z)$. The equation is greatly simplified at high altitudes where $m = 0$. Also in parachute descent the altitudes from 60 to 30 km are covered in approximately 10 min so that sec z is essentially constant for low z.

Equation 5 is strictly true only if the ozone concentration is approximately constant with height. Above the primary ozone peak the concentration decays roughly exponentially with height and a correction can be applied to obtain the true concentration, $\varepsilon(h)$. In this case,

$$\varepsilon(h_o) = -\frac{\Delta x/\Delta h}{H\left[\exp\left(-\frac{\Delta h}{H}\right) - 1\right]} \quad (6)$$

where h_o is the base of the altitude interval, Δh, and H is the ozone scale height (assumed constant over Δh).

ROCOZ SYSTEM DESIGN

FLIGHT CHARACTERISTICS

Atmospheric soundings using the Arcas rocket generally use a dropsonde technique. The rocket carries a payload to an altitude of 55 to 65 km where a gas generator ejects the payload for deployment on a parachute. As mentioned earlier, the relatively slow rate of descent allows a longer time for measurement than would be obtained in free fall. (A typical height vs. time profile is shown on page 26.) The rocket is launched from a closed-breech tube that creates an initial speed of 150 ft/sec to decrease wind effects on the motor-case impact location. A 200-msec launch shock peaking near 60 g is found. The motor burns for 28 sec giving the system an acceleration of 4 to 5 g. At burnout a 100-sec pyrotechnic delay train is initiated that, in turn, ignites the ejection mechanism near apogee. The ejection system produces a brief 70-g shock.

A 15 ft metallized silk parachute has generally been used with this system. The descent rate is proportional to air density, varying from 135 m/sec at 55 km to 20 m/sec at 30 km. During this portion of descent a high amplitude pendulation is observed. This is due to an initial 1,200-rpm spin required for rocket stability and the parachute characteristics. The pendulation is gradually damped out by aerodynamic drag and internal friction in the parachute. Below 30 km pendulation due to wind shears is observed.

Scientific data from the payload are generally transmitted on a 1680-mHz carrier to a GMD meteorological receiver. Information on altitude and winds is obtained by a tracking radar.

DESIGN CRITERIA

The basic task is to design a multichannel ultraviolet filter photometer, capable of stable operation in the environmental conditions set by the rocket flight followed by slow parachute descent through the atmosphere. In addition to mechanical conditions stated above, the payload must incorporate thermal insulation as it is exposed to atmospheric temperatures ranging from +30°C to -80°C. The package design is thus somewhat restricted.

A second criterion has been the cost of expendables. The general rule has been that the payload cost should not exceed the vehicle cost by a large margin. Because system-use costs also involve data readout and reduction, a great advantage is gained by automatic digitizing of the data. For this reason the system has been designed as a point sampler, incorporating a signal that allows direct real-time digitization of the signal. The optical sampling rate is determined by the desired point vs. height density and the maximum descent rate. Given a minimum point density of 5 per kilometer, one sample per second of each optical channel is required from the flight profile.

A third criterion is field serviceability. The payload is designed for convenient disassembly and reassembly for replacement of modular components while maintaining optical alignment.

FLIGHT INSTRUMENT DESIGN

The ozonesonde is designed as a sequential sampling filter photometer. It makes use of a standard meteorological frequency and ground station for telemetry but requires specialized equipment for data recording on the ground. To provide flexibility in channel capacity and bandwidth, subcarrier oscillators and CW modulation have been utilized.

A block diagram of the sounding payload is shown in Fig. 4. In order to obtain the required data point density consistent with data readout capability, an automatic digital recording system has been constructed with real-time capability.

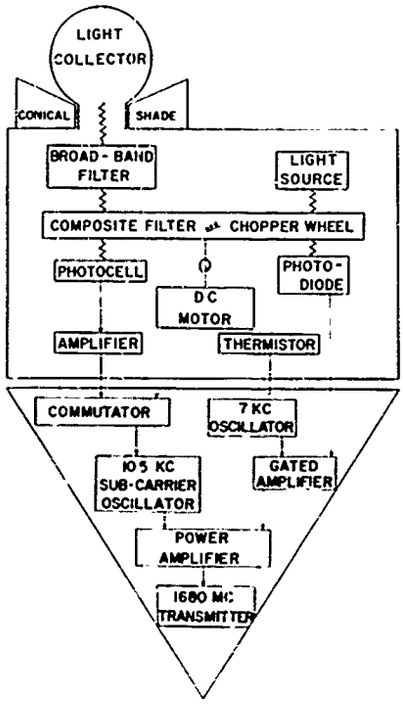

FIG. 4. Block Diagram for ROCOZ Ozonesonde.

PHOTOMETER CONSTRUCTION

Integrating Sphere. To avoid the complexity of an active pointing system the photometer has been designed to accept light from a wide angle field of view. The optical system is adapted from that used in the Paetzold ozonesonde. As in that instrument a transmission-type integrating sphere accepts light from all unobscured angles. The device consists of a hollow Suprasil sphere, open on the base, and internally coated with an optically thick layer of magnesium oxide. Light incident on the surface of the spherical portion is scattered by the magnesium oxide coating. The portion that is scattered into this sphere is internally scattered and finds its way to the photometer entrance aperture. The light available for the photometer is dependent geometrically on the illuminated surface area. For a sphere this is independent

of the angle of incidence so the performance is controlled by the quality of the magnesium oxide coating. A properly constructed sphere has a homogeneous coating with a direct ray transmission of 0.01 to 0.05% and a net transmission of 1% to 2%.

With a semi-isotropic receiver, at some altitude the scattered light becomes a measurable fraction of the total light and a correction becomes necessary depending on the wavelength. Because most of this light comes from angles near and below the horizon, a shield limiting the field of view to elevation angles greater than either 20 or 30 degrees has been installed. This has a second function of protecting the sphere during the payload ejection sequence.

Optical Filters. The optical filters are physically divided into two sections: (1) a broad-band filter that serves to isolate the ultraviolet region of interest and effectively block the visible region, and (2) a set of four narrow-band filters that define the particular bands of interest. The broad-band filter consists of 12-mm $NiSO_4 \cdot 6H_2O$ sandwiched between 3-mm plates of Corning 9863 glass. An absorbance curve of a representative filter is shown in Fig. 5.

The narrow-band filters are composite interference and chemical filter assemblies constructed to have half-widths of 40-50 Å centered near 2700, 2950, 3050, and 3300 Å. Transmission curves for a representative set are shown in Fig. 6. At the present time these filter sets are constructed in-house using commercial components where available. Primary criteria are center wavelength, half-width, and equivalent band pass or peak transmission. The latter parameter is determined such as to provide equal signals from all filters outside the ozone region (h > 60 km).

The narrow-band filters are installed in a five-position filter wheel in which one position is filled with an opaque insert. This wheel is rotated continuously at 60 rpm by a Brailsford motor mounted inside a magnetic shield to minimize radiation. The optical components are shown in Fig. 7.

Photodetector Selection. The types of photodetectors available for use in the near ultraviolet are unfortunately very limited. Photomultipliers and vacuum photodiodes are bulky and expensive but are quite desirable in terms of dynamic range and linearity. Of the solid-state photodetectors only special selenium photocells and some varieties of silicon cells have residual sensitivity down to 2500 Å. The small sensitive area of the silicon cells makes them unattractive. Selenium photocells are available in a range of sizes with quartz cover plates. These cells suffer from the same shortcomings of other solid-state photodetectors: relatively long time constants and temperature coefficients. Because of the extreme cost and volume advantages of the selenium photocell over vacuum phototubes and photomultipliers it was believed that these should be used if possible.

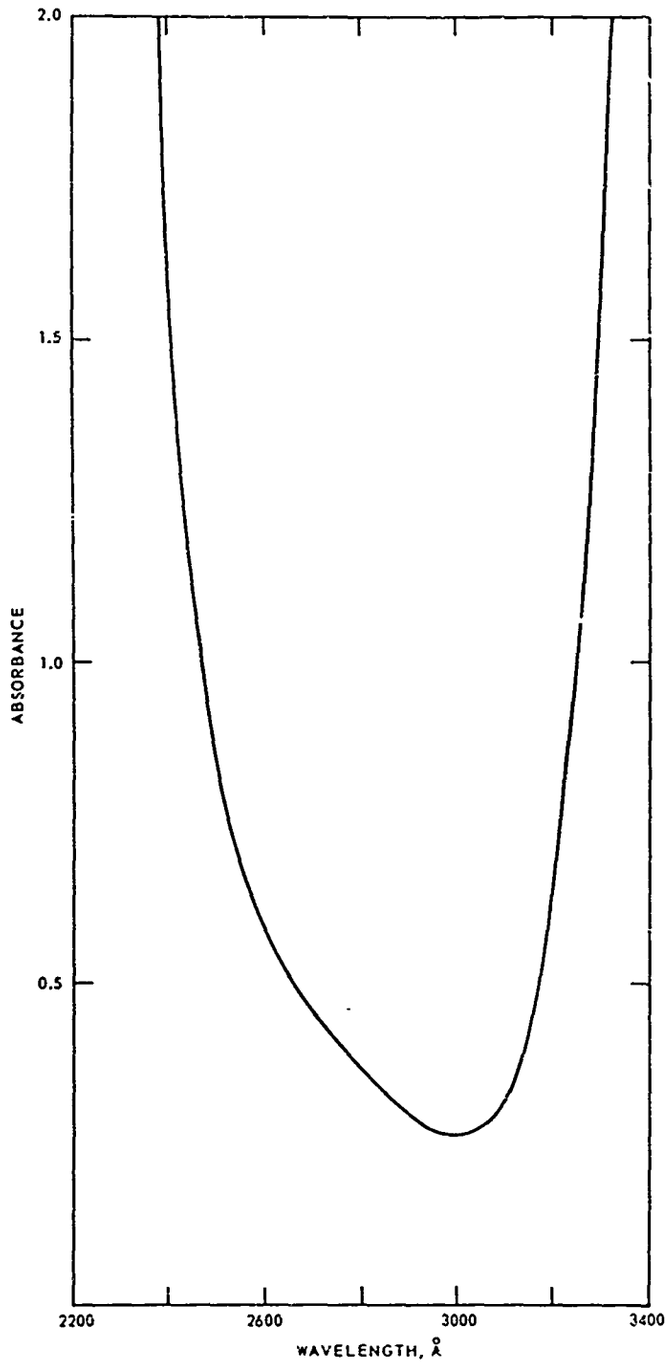

FIG. 5. Absorbance Curve of a Broad-Band Filter.

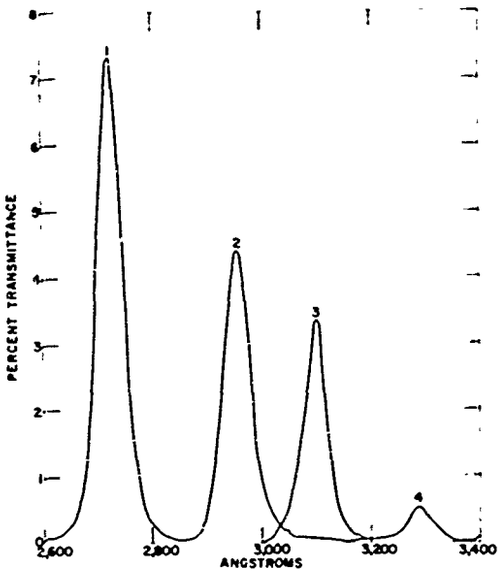

FIG. 6. Transmission Curves of Narrow-Band Filters.

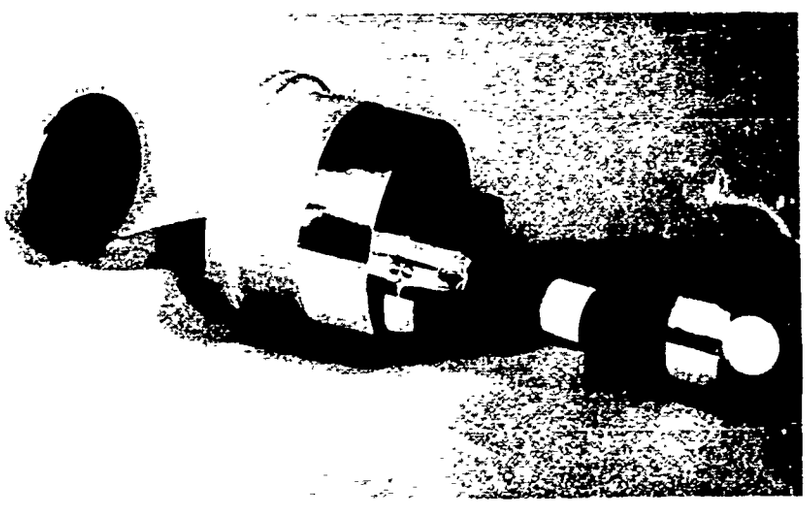

FIG. 7. Optical Components.

When selenium photocells[1] are loaded by a low-input-impedance amplifier, linear response is obtained with low-frequency signals. Response of the cells to a varying signal can be described by two characteristic time constants, one determined by the cell capacitance and the load resistance, and the other a fixed internal characteristic of the cell. The load impedance can be made low enough so that the first time constant is small compared to the sampling rate. A suitable compensation is applied to the data to remove the effects of the internal time constant.

Photometer Amplifier. Photocell signal currents are on the order of 2×10^{-9} amp and, as stated above, a basic requirement for linearity is a low load impedance. An operational amplifier used in a current-to-voltage converter mode is capable of supplying the gain with low input impedance. Because of the temperature range encountered during the flight the drift requirements are severe. A limit of 4×10^{-12} amp/°C is required to limit output change to 0.1 v over this temperature range. This performance is available from a negative feedback transistor amplifier with a capacitive coupling to the input. Although DC response cannot be obtained, with a band pass from 0.01 to 20 Hz a suitable compensation can be applied to the data to recover the pulse levels in a quasi-steady-state situation. The method of compensation is described in the Appendix.

ASSOCIATED PAYLOAD COMPONENTS

Telemetry. The photometer output signal is fed to a standard subcarrier oscillator (voltage-controlled-oscillator) with a 10.5 kHz center frequency. That output is suitably amplified and modulates the transmitter, which is of the type used in meteorological rocket sounding payloads. The frequency is 1,680 mHz. A spiral helix slot antenna is used to give a reasonably isotropic radiation field.

Package Temperature. To monitor the photometer sensing head temperature during flight a bead thermistor is installed behind the photocell. It is part of a shunted voltage divider that has an output voltage in the range of 0 to 5 v. This temperature is sampled for 1.5 sec every 5 min by an electronic commutator in the photometer signal circuit.

Marker Pulse Generator. To allow for automatic digital recording readout of the telemetered data, marker pulses are generated between each pair of light measurements. The system consists of a micro-

[1] The selenium photocells used for this application were manufactured by Dr. Bruno Lange in Berlin, Germany.

miniature light bulb mounted in the photometer case above the filter wheel. Small holes in the filter wheel allow brief pulses of light to pass to a photodiode. The photodiode is used as a gate to allow bursts of signal from a 7-kHz oscillator to pass to an amplifier. The amplifier output is then mixed with the subcarrier oscillator signal.

Power Supply. For primary power four 3-amp-hr-silver-zinc cells are connected in series. The electronic components require +28, -28, and +125 vDC. These are supplied by a DC-to-DC converter. The transmitter filament, filter wheel motor, and miniature light source are supplied directly from the primary power source.

PHYSICAL CONSTRUCTION

Packaging and Thermal Control. All components are stacked such that the maximum diameter conforms to an extended Arcas nose cone. For thermal stability, shock and vibration control, and component protection, the active assembly, exclusive of photometer sensing head, is potted in a medium density polyurethane foam. To ensure dimensional stability of the potting during upflight this foam is cured at 70°C for 12 to 24 hr. All noncommercial electronic circuits are potted in Eccogel 1265 epoxy resin for thermal and mechanical stability. Figure 8 is a drawing of the completed assembly.

Deployment System. To minimize the problems of obscuration of the sun and backscattered light from the parachute, a device has been constructed to lower the instrument approximately 15 m below the base of the parachute. This device consists of a coil of 3/16-in. nylon rope installed in a deployment can that mounts on the photometer head. At ejection this can stays with the parachute and the instrument falls away until the rope is completely extended.

Ground Station and Digital Data Recording. As noted previously due to the high initial descent rate at altitudes at which data are particularly desirable a high sampling rate is required. In the interest of simplicity the same sampling rate is maintained throughout the flight. This mass of data points is, of course, useful but manual data readout is prohibitively time-consuming. For this reason an automatic digital recording system has been constructed. The demodulated telemetry signal is taken from the GMD meteorological receiver after the detector. A line driver has been constructed for insertion in the socket of the V-1001 modulation amplifier and cathode follower. The signal consists of the frequency-modulated 10.5-kHz subcarrier channel mixed with 7-kHz marker pulses. These frequencies are separated by band pass filters and are fed to a logic assembly (Fig. 9). The marker pulses generate gating pulses that control two parallel counters. One counter accumulates the number of crossovers of a 12.5-kHz-crystal-controlled oscillator in the

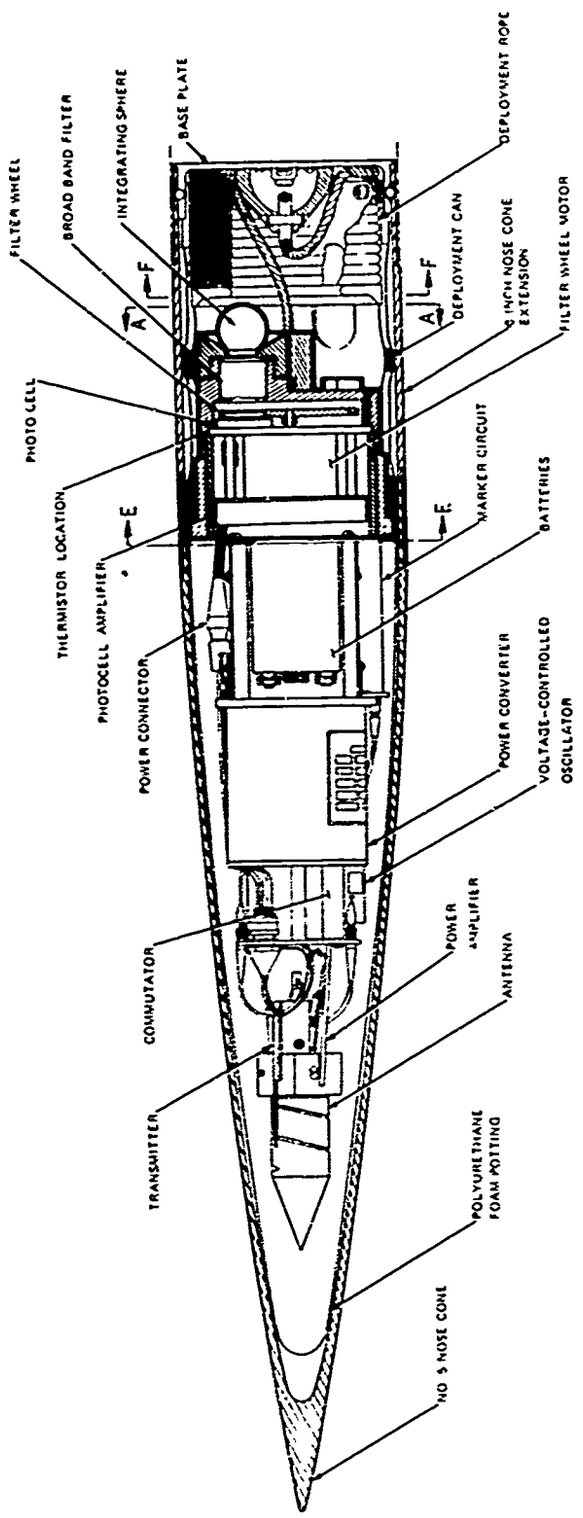

FIG. 8. Completed Assembly.

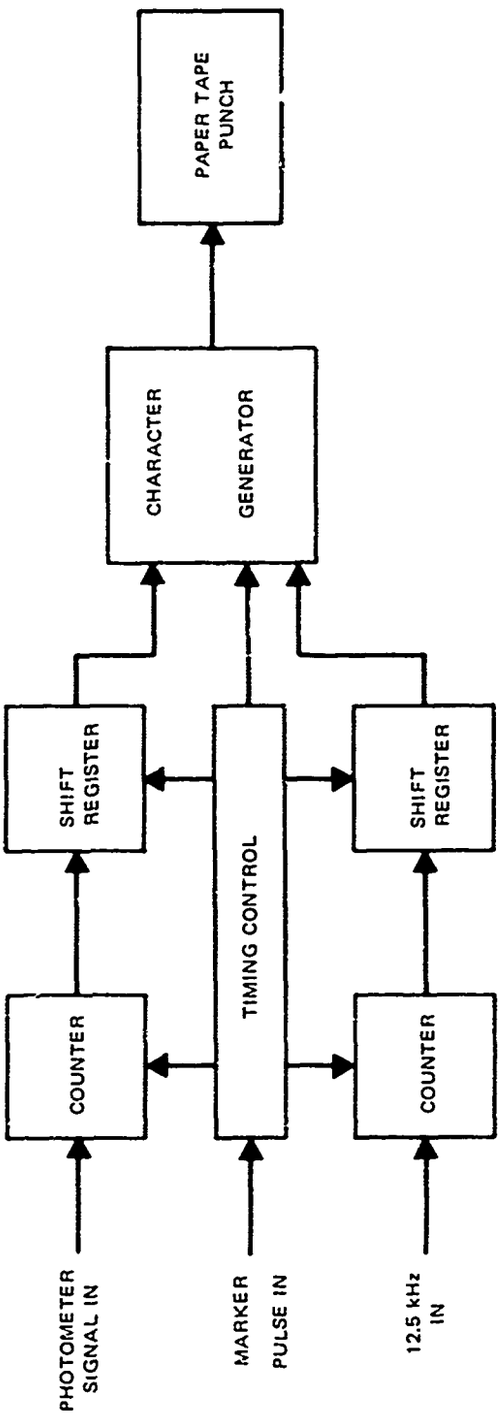

FIG. 9. Digital Data Logging System.

ground station, used as a measure of elapsed time between marker pulses. The second counter accumulates the number of subcarrier crossovers in the same interval. During the marker pulse the previous counts are transferred to storage registers, the counters are reset to zero, and a new count begins. As the new count is accumulating, the previous time and data words are serialized and punched out on paper tape together with a parity channel and flags to indicate time or data words. In order to provide a continuous time count so that elapsed time from launch can be maintained in relation to real time an automatic dump mode is available. This is required due to dropouts in the telemetry signal that occur on the upflight and after ejection before the parachute-payload system stabilizes. In the automatic dump mode if a marker pulse is not received before the time counter fills up to a present level a dump to the tape punch is made and an unique flag is punched.

Auxiliary systems consist of a discriminator and strip-chart recorder for in-flight monitoring of performance and an analog tape recorder on which is recorded the raw demodulated telemetry data, the 12.5-kHz timing frequency, a standard real-time code, and voice annotation. The discriminator serves a dual purpose in that the channel band-pass filter serves as the data channel filter for the digital system.

This type of digital data recording system has the advantage of high frequency noise rejection because of integration over a number of cycles that average to zero. Disadvantages are sensitivity to impulse noise and telemetry dropouts.

DATA ANALYSIS

The procedure for reduction of ROCOZ flight data to ozone distribution is lengthy and is the primary shortcoming of the optical technique. However, because the method yields absolute ozone concentrations, albeit with smoothing over any detailed structure, the task must be considered worthwhile.

A flow chart of the complete analysis process, including calibration is shown in Fig. 10. Although it is possible to handle all steps in a computer, at this time only a certain number have been programmed. These are the steps involving the most data handling.

The flight-data reduction process starts with either conversion of the punched paper tape generated in flight to a computer-compatible digital tape or by digitization of the analog tape. This digital magnetic tape contains only the crossover counts of the data channel and a reference constant frequency oscillator between marker pulses. To convert these counts to relative irradiance and elapsed time a

second program is required. The inputs to this program are the data tape and the compensation matrix derived from the preflight photometer calibration. Because this matrix is a function of temperature the one corresponding to the average package temperature in flight is selected. The outputs of this program are the crossover counts per unit time for each filter wheel position, the compensated intensity values for the four filters, and the ratios of the absorbed wavelength intensities (2700, 2950, and 3050 Å) to the reference wavelength intensity (3300 Å). These values are stored and listed for each sample together with the elapsed time at the beginning of each frame from the start of the recording.

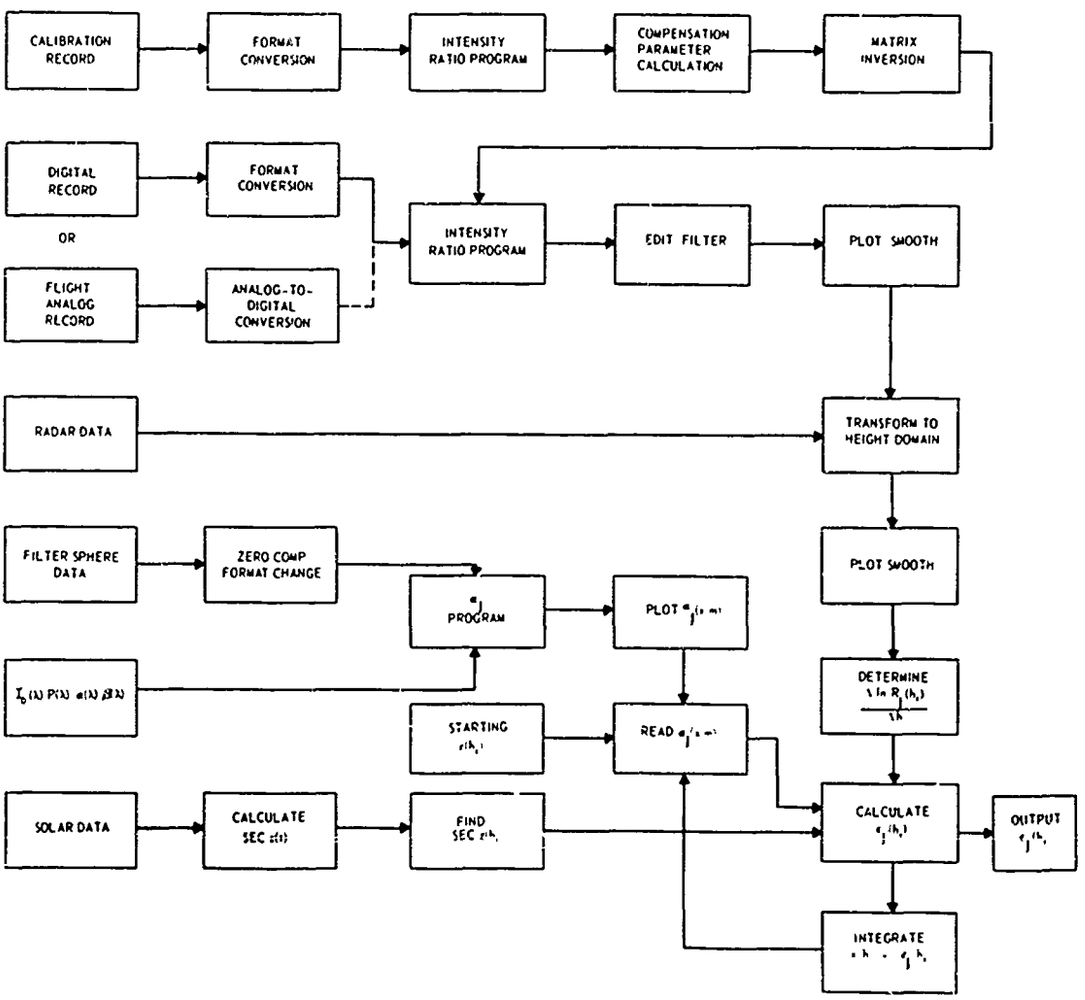

FIG. 10. ROCOZ Data Processing.

The next step in the reduction procedure is to filter the data to eliminate the noise contributions due to system noise and pendulation on the parachute. To assess the filtering parameters as well as to evaluate the over-all operation and compensation, the raw data are plotted vs. time by a computer program. Two filtering routines have been used with ROCOZ data. The first was a low-pass digital filter in which the cut-off frequency and sharpness are adjustable parameters. Because the natural frequency of the intensity vs. height (or time) curve is very low and the mechanics of the system introduces transients in the data, this type of filter was not very successful.

The filter presently being used is a least-squares sliding polynomial curve-fitting routine. It has the advantages of rapid response to transients (which can then be appropriately treated) and a true response to clean data. The output of this filter is presently printed and plotted. It then becomes necessary to decide whether the filtering parameters have been selected correctly and whether additional smoothing is possible or desirable. In general with the present system, because of transients introduced by the dynamics while on the parachute, it is then necessary to manually smooth the filtered data to remove the ficticious transients. The result is intensity vs. time curves for each sampled wavelength.

It is normally most convenient to work with the intensity data as a function of height rather than time. The height vs. time data are obtained independently from a tracking radar and are typically furnished to the user as a computer printout. Irregularities are removed by smoothing a manual plot of the data. Times for crossing selected heights (typically each kilometer) are then read off and used to construct intensity vs. height profiles.

Additional input data required to calculate the ozone distribution are the effective absorption coefficients for each filter, sec z vs. height, and air temperature vs. height.

The effective absorption coefficients, α_j, are calculated using Eq. 3 that has been programmed for integration with a wavelength increment of 1 Å. While this wavelength resolution is greater than is required, the determination of input parameters with fine structure (solar spectrum, ozone absorption coefficient) is made easier in that the curve reader is not required to determine averages over the wavelength increment with great accuracy. It is assumed that reading errors are random.

The values of the input parameters were obtained as follows: The extraterrestrial solar spectrum, $I_0(\lambda)$, was read from a tracing of data obtained by the Naval Research Laboratory[2] on 14 June 1949. This trace

[2] Furnished to us by Dr. R. Tousey.

was read at 1 Å intervals in the range 2650 to 3399 Å. Because the original trace was presented in terms of log I vs. λ a short program was written to convert to $I(\lambda)$ and change to the card format used in the α_j program.

The ozone absorption coefficient values $\alpha(\lambda)$ were read from an expanded scale plot of Inn and Tanaka's (Ref. 1) and Vigroux's (Ref. 6) data and punched on cards in the necessary formats. The 18°C values were used. The Rayleigh scattering (extinction) data could not be obtained in a tabulation suitable for this application so a program was written for calculation from the equation:

$$\beta(\lambda) = \frac{8\pi^3}{3} \frac{[(GF + 1)^2 - 1]^2}{\lambda^4} \frac{D}{N^2} \frac{10^{-6}}{6.4894} M$$

in which

$$G = 10^{-8}\left(6432.8 + \frac{2949810}{146 - \frac{10^8}{\lambda^2}} + \frac{25540}{41 - \frac{10^8}{\lambda^2}}\right), \text{ and}$$

$$F = \frac{P[1 + (0.7870 - 0.0118\ T)10^{-6}\ P]}{960.857(1 + 0.003661\ T)}$$

where

P = atmospheric pressure in millibars
T = atmospheric temperature in °C
D = 1.061, the depolarization factor for air
N = relative number density
M = total air mass in molecules/cm^2

The filter transmission curves are obtained by measurement on a Cary Model 14 spectrophotometer. The transmission values at each wavelength were originally read from the tracings but presently are directly obtained in digital form by use of an analog to digital converter. A computer program has been written to compensate for variations in the 100% transmission level and shifts in the zero level and to convert the punched paper tape output of this device to cards in the appropriate format. A similar technique is used for input of the sphere transmission data.

The photocell spectral response curve was measured in the Cary spectrophotometer by comparison with the fluorescent light of a sodium salicylate coated filter disc. The data being used match with that furnished by Paetzold[3] in the crossover region at the long wavelength

[3] Private communication.

end and have a form similar to published data. As a check on the error possibly involved by use of the wrong curve, the α_j's were calculated using a flat spectral response over the entire wavelength region. The results differed by less than 1% from those obtained with the assumed response curve.

The output of the α_j program is a listing of α_j and $\partial\alpha_j/\partial x$ for a sequence of increments in x and M over the ozone and air mass ranges suitable for each filter. These values are plotted for ease of manual ozone computation.

The values of sec z are calculated from position and time data with reference to the Air Almanac for solar GHA and declination using the equation

$$\frac{1}{\sec z} = \cos z = \cos \text{LHA} \cos \delta \cos \phi + \sin \delta \sin \phi$$

where

ϕ = latitude
δ = solar declination
LHA = GHA-longitude

For use here the values are calculated at convenient times, plotted, and the required values read from this curve. (More recently a computer program has been written for this calculation.)

From these parameters and the intensity distributions the ozone distribution is calculated using Eq. 5. The convergence is rapid, such that only two iterations are required. It is possible to make precise corrections for the ozone absorption coefficient temperature dependence in two cases: (1) when the concentration decreases rapidly with height as above the main peak, and (2) for isothermal regions. Although the techniques for introducing this temperature correction have not been formalized, the present procedure is to evaluate the distribution assuming 18°C ozone, then apply the corrections derived from Vigroux's data. The air temperatures used in this calculation are obtained from independent radiosonde or rocketsonde flights.

The altitude increment size used in the ozone calculation determines the resolution of the distribution. The quality of the intensity data is used as a guide in selection of the minimum increment. Generally, 2 km is used unless data of exceptional quality are obtained.

FLIGHT TESTING

The rocket-test-flight program of the complete system was initiated in December 1963 after several balloon flights of prototype instruments in which optical filter parameters and the mechanical design were evaluated. An earlier rocket flight, in June 1963, was made to test the deployment system. With the exception of a single flight at White Sands Missile Range, the tests were conducted at the Pacific Missile Range (PMR), Point Mugu, California. All flights used the system described in this report except for minor changes in potting procedures.

The ground station for the earlier flights consisted basically of an analog tape recorder, crystal-controlled oscillator, discriminator, strip-chart recorder, and a switching panel. This system was used for primary recording until the digital recorder became available later on in the test series. At that time its use was continued for back-up purposes. Tape recorder channel functions were voice annotation, IRIG B timing signal, telemetry signal, and 12.5 kHz signals. The strip-chart record was used to monitor in-flight performance.

During the entire flight series the analog tape records were digitized using the data automation system at this Center. For conversion of the real-time punched paper tapes to computer-compatible magnetic tapes, a program was written by PMR Weather Center personnel for use on their meteorological computer. These tapes were then returned to China Lake for further reduction.

A listing of test flights and various performance characteristics is given in Table 1. This program suffered greatly from rocket problems with three motor malfunctions out of the 11 flights. After higher quality rockets were obtained problems in the transmitter and payload potting procedures resulted in further failures. These problems were resolved in the final flight in October 1964. An analysis of this flight is given in the next section of this report. Although this flight was made with less than optimum solar zenith distance conditions, it was possible to examine the system performance and derive an ozone distribution.

Shortly after the test flights were completed, a series of flights was made from the U. S. S. Croatan on the NASA Mobile Launch Expedition #1. From these nine flights it is possible to make a realistic estimate of the package reliability and set certain conditions for its use. Of these flights, one rocket motor and one ground station (GMD) failure occurred. Of the payloads, one transmitter failed due to over-heating during an extended prelaunch hold and an integrating sphere was broken in another flight. The net result was five successful flights out of nine launches.

TABLE 1. ROCOZ Test Flight Summary.

Flight no.	Location	Date	Launch time	ROCOZ	Vehicle	Max. alt., ft	Vehicle operation	Payload operation	Payload changes
6	Ely, Nev.	10 23 61	0925 MST	1	Balloon, 69-ft dia.	°	Good	Power system failure	
7	Ely, Nev.	10 25 61	0854 MST	2	Do.	°	Good	Power system failure, no modulation	
8	Ely, Nev.	1 29 62	1115 MST	2	Do.		in-flight failure		Thermal insulation
9	Ely, Nev.	1 31 62	1000 MST	1	Do.	101,000	Good	Good	Commutated marker pulse
17	Ely, Nev.	7 30 62	0954 MST	3	Do.	100,000	Good	Good	
19	Ely, Nev.	8 1 62		4	Do.		No flight, launch accident		
28	Pt. Mugu, Calif.	6 12 63	0955 PST	dummy	ARCAS Rocket	209,000	Good	Deployment system test, good operation	
31	Sioux Falls, S. Dak.	8 31 63	1110 CST	5	Balloon, 3.5 × 10^6 ft^3	147,000	Good	Okay, but noisy data	AM marker system
32	Pt. Mugu, Calif.	12 19 63	1134 PST	6	ARCAS Rocket	191,000	Good	First rocket test, low modulation level	Full rocket assembly
33	Pt. Mugu, Calif.	2 12 64		8	Do.		Rocket blowup		Modulation level change
34	White Sands, N. M.	3 16 64	1305 MST	7	Do.	?	No radar track	Separation from parachute	
35	Pt. Mugu, Calif	6 10 64	1120 PDT	10	Do.		Rocket blowup		
36	Pt. Mugu, Calif.	6 11 64	0855 PDT	11	Do.		Rocket blowup		
38	Pt. Mugu, Calif.	7 9 64		dummy	Do.	178,000	Good, test of new series		
39	Pt. Mugu, Calif.	7 10 64		9	Do.	173,000	Good	Transmitter failure at ejection	
40	Pt. Mugu, Calif.	7 23 64	1505 PDT	10	Do.	178,000	Good	Transmitter failure, upflight	
42	Pt. Mugu, Calif	8 19 64	1020 PDT	12	Do.		No launch	Transmitter failure, on pad	
43	Pt Mugu, Calif.	8 26 64	1207 PDT	12	Do.	165,000	Low apogee	Good, nose cone stuck	Transmitter potting
44	Pt. Mugu, Calif.	10 7 64	1431 PDT	11	Do.	170,000	Good	Failed at ejection, separated from parachute	Potting cure change
45	Pt. Mugu, Calif.	10 8 64	1042 PDT	13	Do.	163,000	Low apogee	Good	

° Telemetry lost.

ANALYSIS OF DATA FROM FLIGHT 45

The final flight in the test series, NWC Flight 45, was launched at PMR on 8 October 1964 at $17^h\ 40^m\ 58^s$ GMT with a solar elevation angle of 41 degrees. The flight operations were conducted by the Geophysics Division of PMR. Peak altitude achieved was 163,000 ft (49.8 km) which, for the payload weight, is somewhat lower than nominal 180,000 ft (55 km). Figure 11 shows the altitude vs. time for this flight. Optical signals from the photometer were received within 0.2 sec after ejection that took place at 1743 hr. The parachute opened 1.4 sec after ejection and a clean photometer signal was received. This signal during the ejection and deployment sequence is shown in Fig. 12. The data frames, consisting of pulses from the four filters and a zero level, showed variability in relative pulse height due to the rapid rotation of the payload soon after ejection. Within 10 sec after ejection a longer period modulation of frame amplitudes also appeared. This modulation was regular with an initial period of 8 sec and amplitudes up to 80%. The modulation continued with high amplitude until 1811 hr. Because of the low solar elevation angle, pendulation angles exceeding 11 degrees would result in modulation of the type observed. An increase in amplitude of the 3050- and 3300-Å pulses occurred at 1750 hr such that clipping of the highest pulses took place until 1802 hr. Telemetry was generally clean throughout the flight although large fluctuations in the RF signal strength were observed initially, decreasing as the package descended. The data were recorded on analog magnetic tape and, using the logic system, on punched paper tape in digital form. Because of the signal strength variations some difficulty was noticed in maintaining the proper level for triggering of the logic system by the marker pulses.

The package temperatures were read out from the in-flight analog strip-chart record and are shown in Fig. 13. A 27°C total change was observed, but during the portion of the flight in the primary ozone region above 20 km the changes are limited to 11°C. For this reason the compensation matrix for room temperature was used for the data readout.

Two methods of digital data readout were used to provide a comparison of real-time analog and digital recording. The analog magnetic tapes were processed by the data automation system at this Center. The punched paper tapes were read and processed in part by the PMR Geophysics Division computer personnel. No useable data could be obtained from either source prior to 1800 hr due to excessive modulation of the optical signal and loss of marker pulses during weak portions of the telemetry signal. The data from the analog magnetic tape were significantly lower in quality than that from the punched paper tape. From an examination of the analog strip-chart records it appears that useable data can be obtained from the

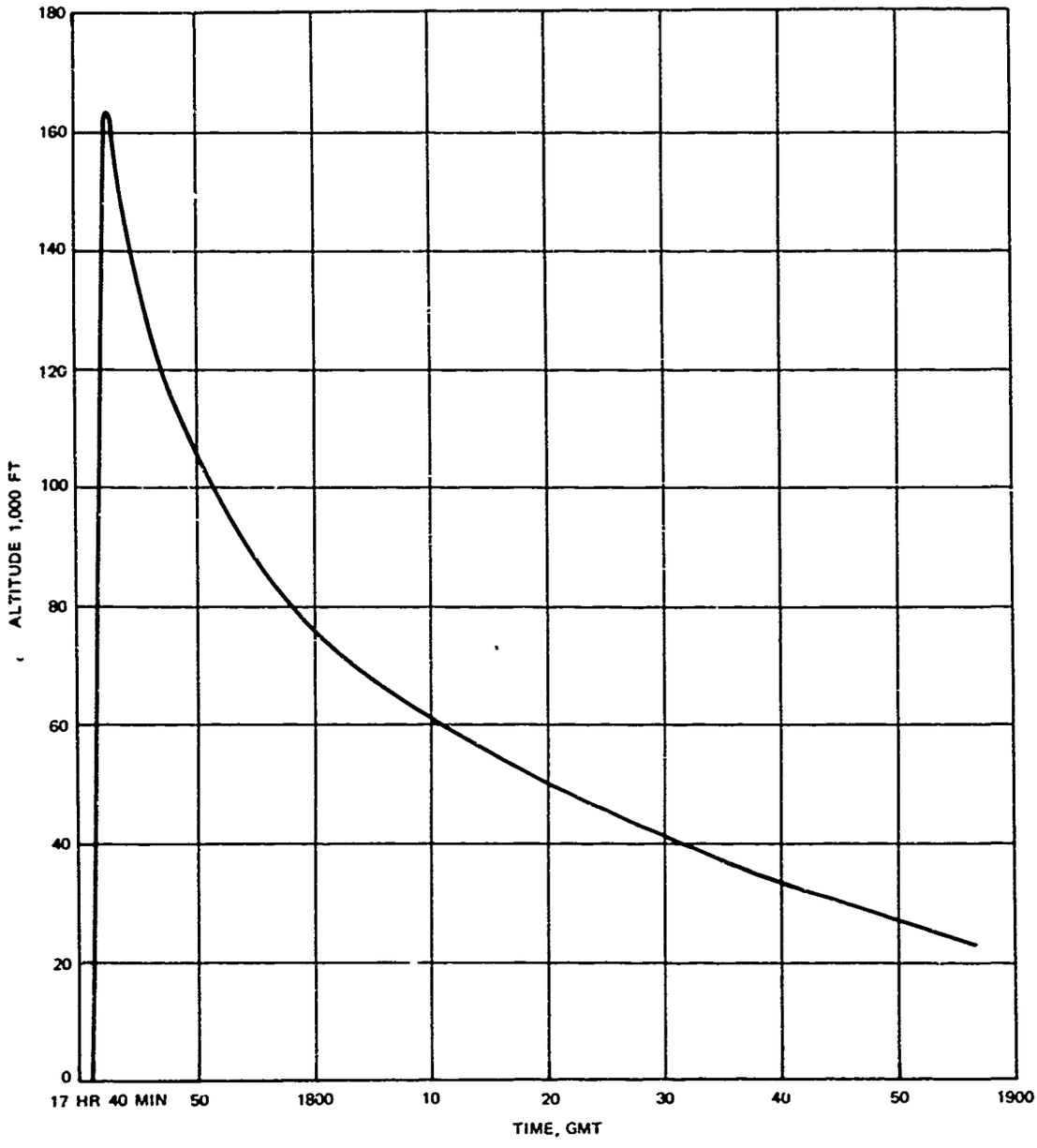

FIG. 11. Altitude vs. Time for Flight 45.

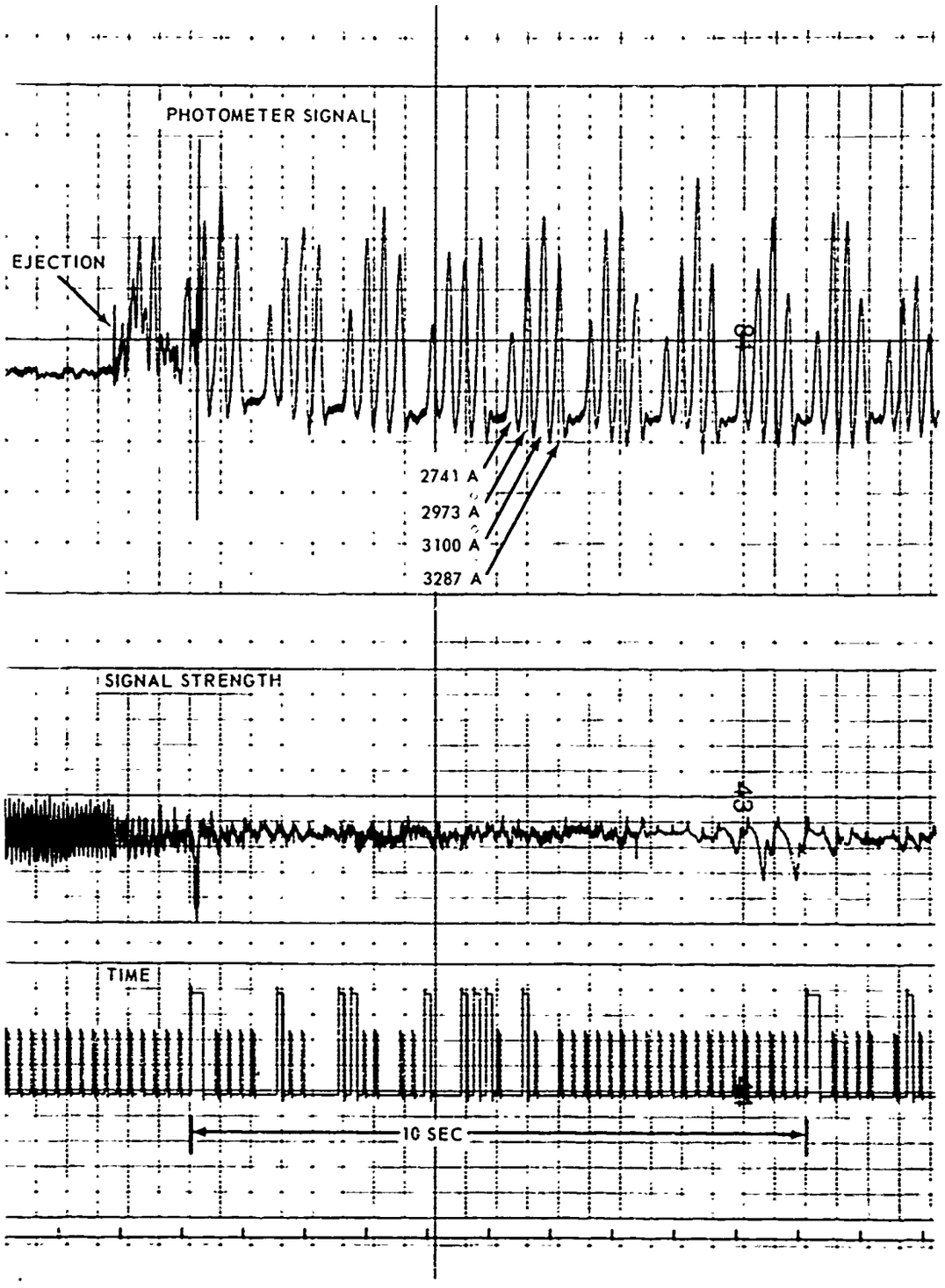

FIG. 12. Photometer Signal During Ejection and Deployment Sequence.

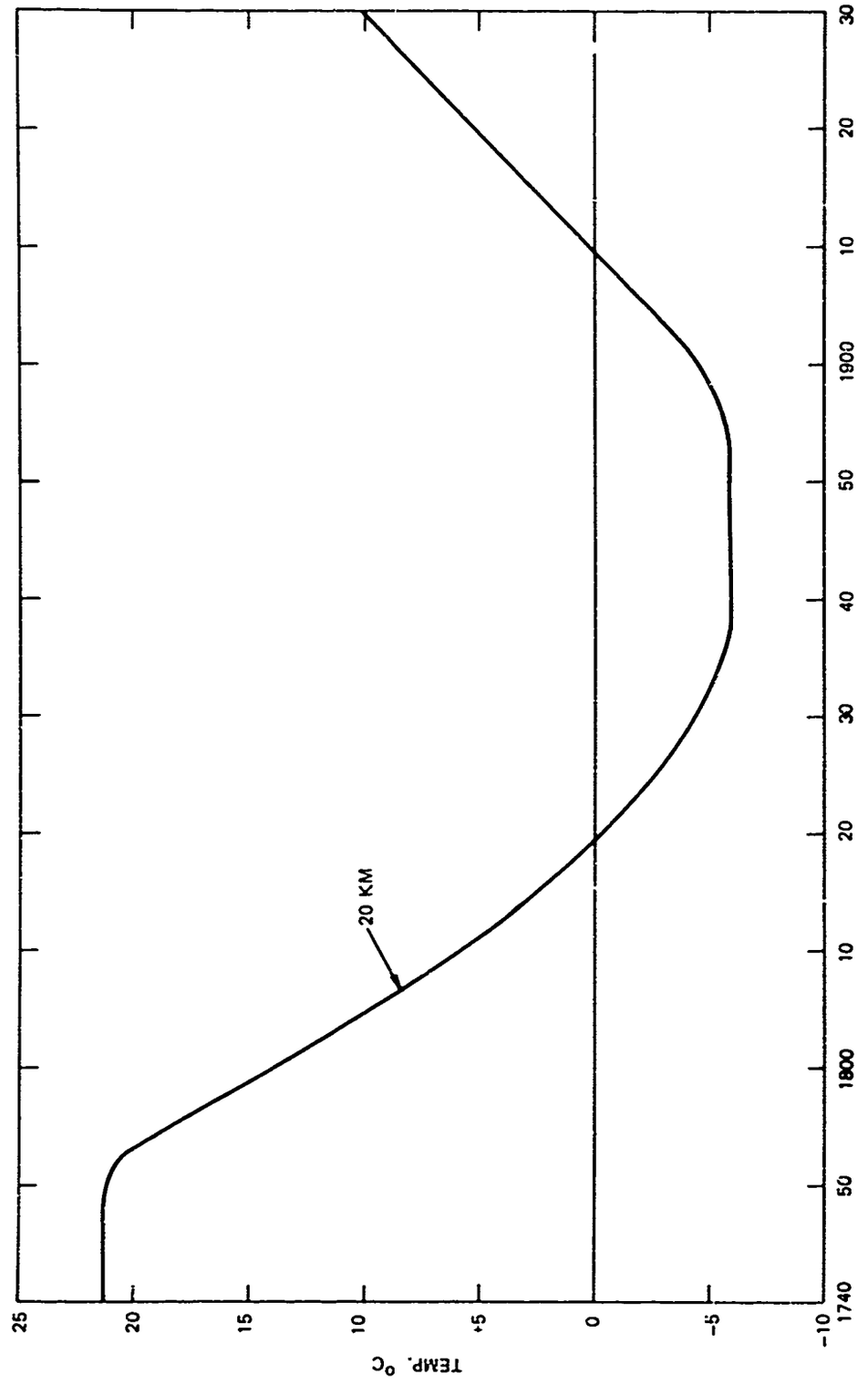

FIG. 13. Package Temperatures.

real-time digital records when the modulation of the light on the photometer is less than 30% in amplitude (i.e., the steady-state approximation holds under those conditions). For greater modulation levels the compensation method diverges.

To obtain intensity vs. height data at higher altitudes the amplitudes of selected pulses on the strip-chart record were measured manually. Smooth curves have been fit to these points. The results are given in Fig. 14 where the light intensities at the three shortest wavelengths relative to the reference wavelength are shown. The clipping problem resulted in loss of data in the 20 to 30 km region.

The characteristics of the optical filters used for this flight are given in Table 2. The listed parameters are center wavelength, λ_c, width at the 50% relative transmission points $\Delta\lambda_{\frac{1}{2}}$, peak transmission τ_{max}, effective band pass $\Delta\lambda_j$, observed and calculated extraterrestrial signal from the photometer relative to the 3300 Å signal S_j/S_o. The discrepancy between observed and calculated ratios has not been explained.

TABLE 2. Optical Filter Parameters

j Filter No.	λ_c, Å	$\Delta\lambda_{\frac{1}{2}}$, Å	τ_{max}	$\Delta\lambda_j$, Å	S_j/S_o obsd.	S_j/S_o calcd.
0	3287	47	0.0041	0.193	....	....
1	3100	48	0.0267	1.28	1.18	3.93
2	2973	54	0.0301	1.62	0.97 (est.)	3.41
3	2741	50	0.0738	3.70	....	2.05

The effective ozone absorption coefficients vs. total ozone amount for this filter set are shown in Fig. 15. The slight influence due to Rayleigh scattering is shown by the curves for different values of m, the relative air mass above the instrument. Here, only the influence of single scattering is taken into account. The absorption coefficients are computed for ozone at 18°C. Especially in the lower stratosphere the ozone temperature, assumed in equilibrium with the air, is significantly lower than 18°C. The temperature dependence of the ozone absorption coefficient is on the average a slowly changing function of the wavelength and a multiplicative temperature function can be used for each filter.

The ozone concentrations were calculated using Eq. 5 and the associated slope correction (Eq. 6). The value of sec z ranged from

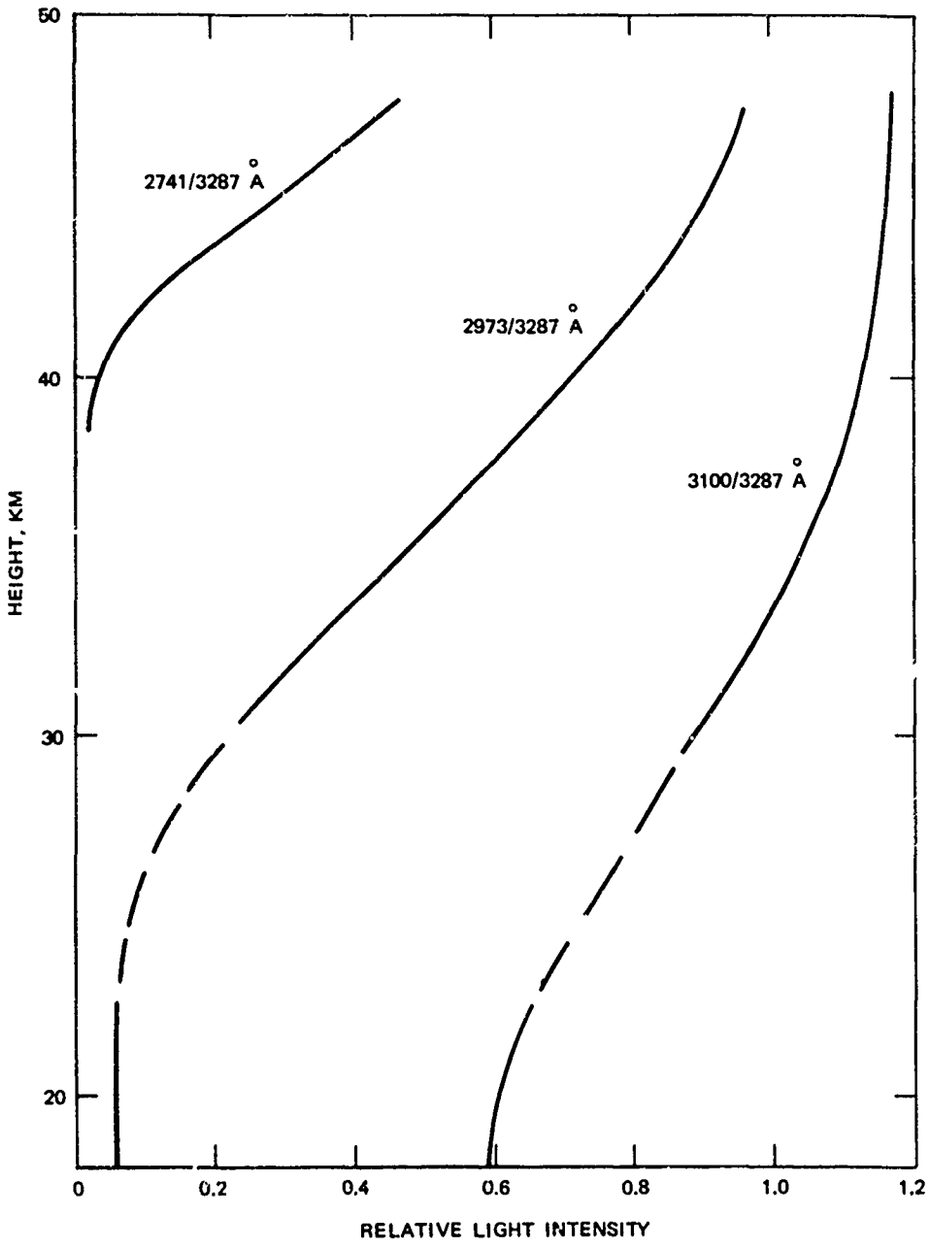

FIG. 14. Intensity vs. Height Data at Higher Altitudes.

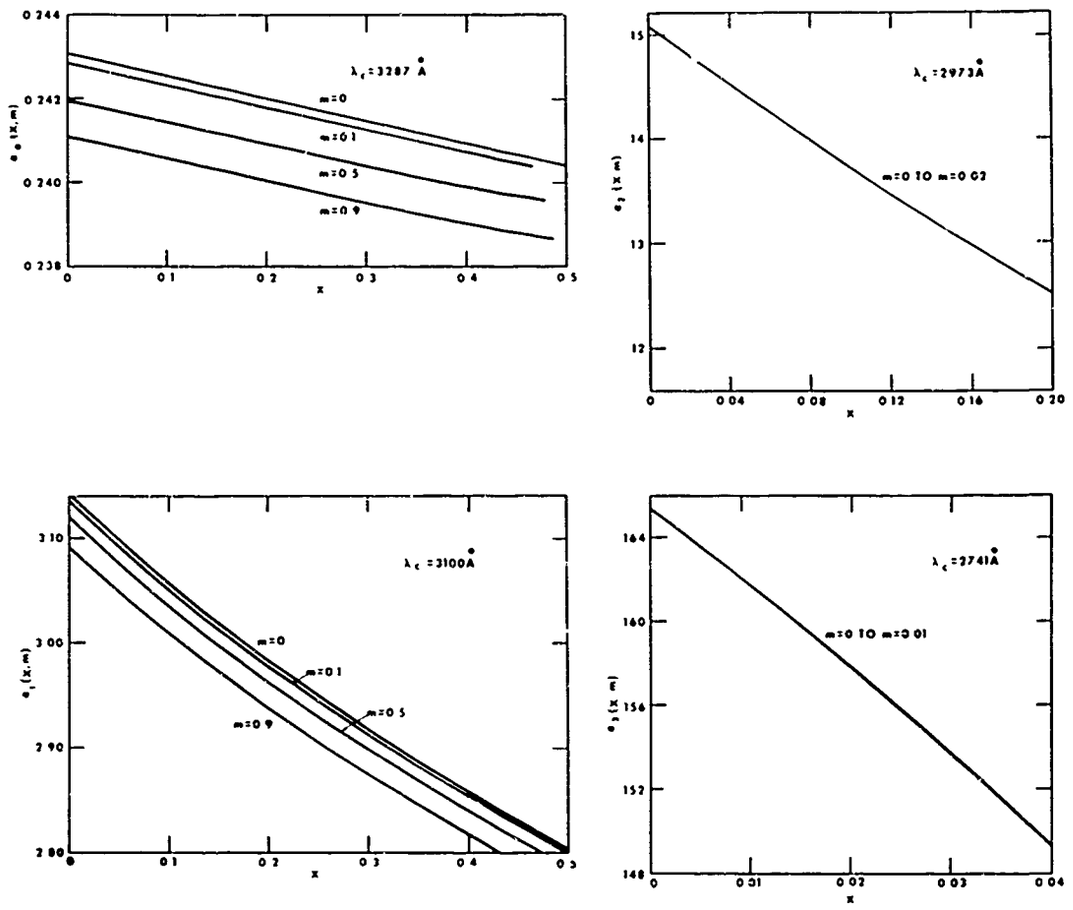

FIG. 15. α_j Curves.

1.527 at launch to 1.456 at 22 km. Considering the data quality an altitude increment of 2 km was selected. Evaluation was not attempted below 30 km because of the previously mentioned clipping problem. Results are shown in Fig. 16. Also plotted are the results of an earlier measurement at White Sands Missile Range on 14 June 1949 as corrected by Craig (Ref. 8). A detailed error analysis has not been conducted at this time; however, an estimate can be made from the concentrations derived from two filters at the crossover region. In this case, at 43 km a 22% difference exists. It is expected that better agreement will be obtained under more optimum flight conditions.

The results of this flight demonstrate that (1) the basic system can operate successfully, (2) the payload-parachute system must be stabilized to acquire digital data and higher quality analog data over the entire altitude range, and (3) the real-time digital recording system produces higher quality data than a digitized analog magnetic tape system.

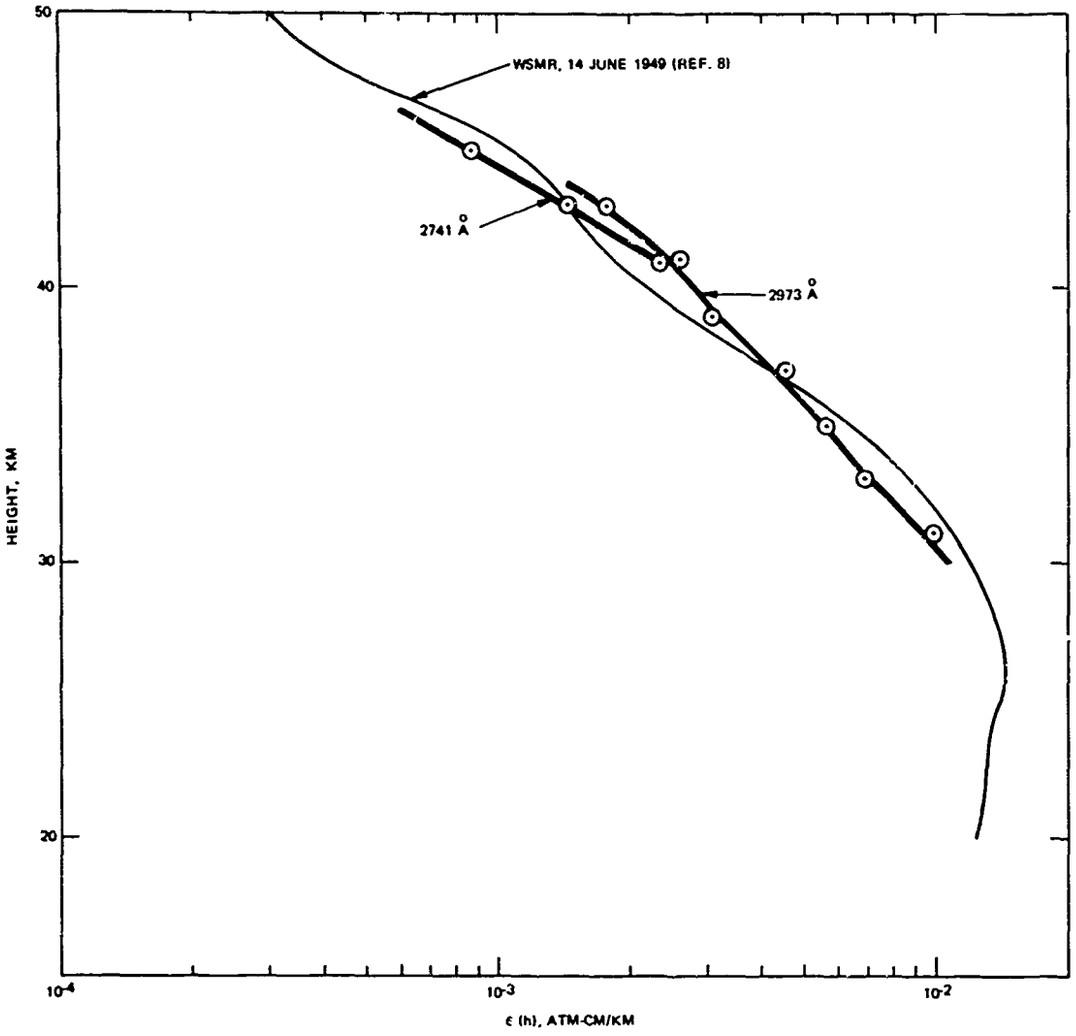

FIG. 16. Ozone Concentrations. Comparison of measurements from Flight 45, 8 October 1964 at Point Mugu, Calif., with earlier measurements from White Sands Missile Range, N. Mex.

Appendix

LINEAR OVERSHOOT MODEL OF AMPLITUDE COMPENSATION

In the ROCOZ system the irradiance in four narrow spectral bands and a zero light level are sampled sequentially. Each group of five samples is denoted a frame and for steady-state illumination conditions the frames are identical and occur repetitiously. The time variation of the irradiance in each pulse at the photodetector is determined by the system geometry and consists of a symmetrical pulse with a rounded top. In a direct-coupled system with a fast-response detector the individual pulse amplitudes or the pulse areas serve as a measure of the irradiance when referred to the zero light level value.

In this application, due to cost and physical space considerations, the use of a solid-state photodetector is desirable. This device has internal time constants of the same order of magnitude as the sampling period that is determined by flight parameters. A further complication arises from the low irradiance levels available. Due to the small signal currents, suitable direct-coupled amplifiers with satisfactory drift specifications have not been available until recently.

It has, therefore, been necessary to derive a method for compensation of the observed signals to obtain the input irradiances. Although the method is illustrated with analog wave forms, it is applied to a discrete set of measurements that consist of the areas under the pulses. Each pulse is characterized by its position, i, in the k^{th} frame. Residual effects persisting after the input pulse has gone to zero are characterized by the integer j equal to $n\Delta i$.

An input pulse of light, $I_{k,i}$, is transformed by the photocell and amplifier to the output pulse

$$S_{k,i,j} \equiv Y_{k,i,j} - A_{k,i}$$

where $A_{k,i}$ is the average signal level over one or more frames preceding the sample $I_{k,i}$ (Fig. 17).

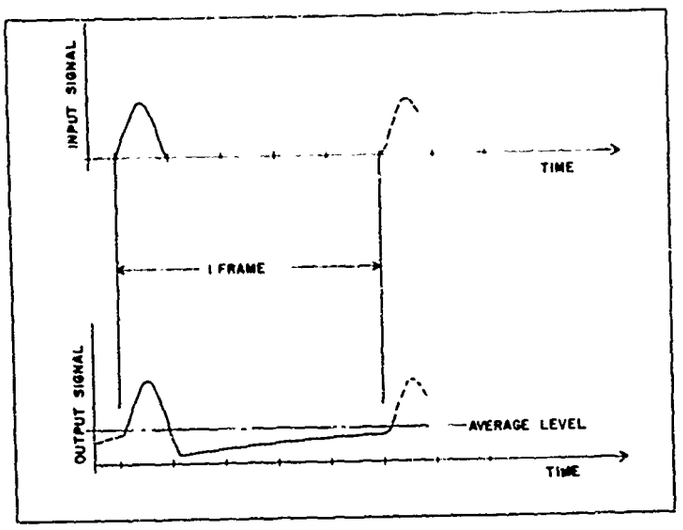

FIG. 17. Amplifier Overshoot Characteristics.

Each output pulse is modified by the preceding pulses such that

$$S_{k,i,0} = BI_{k,i} - S_{k,i-1,1} - S_{k,i-2,2} - S_{k,i-3,3} - \cdots$$

$$= BI_{k,i} - \sum_{j=1}^{n} S_{k,i-j,j}$$

where if $j>i$, set $i-j \rightarrow i-j+5$ and $k \rightarrow k-1$, and B is defined as a sensitivity constant. In a steady-state situation, it is obvious that $S_{k,i,j} = 0$ for $j>4$ for a five sample per frame device. Thus in this case there is the following set of equations

$$S_{k,0,0} = BI_{k,0} - S_{k-1,4,1} - S_{k-1,3,2} - S_{k-1,2,3} - S_{k-1,1,4}$$

$$S_{k,1,0} = BI_{k,1} - S_{k,0,1} - S_{k-1,4,2} - S_{k-1,3,3} - S_{k-1,2,4}$$

$$S_{k,2,0} = BI_{k,2} - S_{k,1,1} - S_{k,0,2} - S_{k-1,4,3} - S_{k-1,3,4}$$

$$S_{k,3,0} = BI_{k,3} - S_{k,2,1} - S_{k,1,2} - S_{k,0,3} - S_{k-1,4,4}$$

$$S_{k,4,0} = BI_{k,4} - S_{k,3,1} - S_{k,2,2} - S_{k,1,3} - S_{k,0,4}$$

DETERMINATION OF THE OVERSHOOT COMPENSATION PARAMETERS

The compensation parameters $S_{k,i-j,j}$ ($j \neq 0$) could, in principle, be determined from the transfer function of the photometer[4] but in practice an empirical approach has proved useful.

Five input light pulses of known amplitude are fed to the photometer. Consider the simple case where $I_0 = I_1 = I_2 = I_3 = 0$ and $I_4 = I$. The subscript k has been deleted because in a steady-state situation all frames are identical. The value of I is set at various values throughout the useful range of operation.

It is assumed that the overshoot amplitude depends only on the amplitude of the initiating pulse and that the overshoot from a zero amplitude pulse is zero. The five equations reduce to

$$S_{0,0} = -S_{4,1}$$

$$S_{1,0} = -S_{4,2}$$

$$S_{2,0} = -S_{4,3}$$

$$S_{3,0} = -S_{4,4}$$

$$S_{4,0} = BI_4$$

If it is also assumed that the overshoot values do not depend on the position of the originating pulse in the frame, then

$$S_{0,0} = -S_1 \equiv -\Delta_1$$

$$S_{1,0} = -S_2 \equiv -\Delta_2$$

$$S_{2,0} = -S_3 \equiv -\Delta_3$$

$$S_{3,0} = -S_4 \equiv -\Delta_4$$

$$S_{4,0} = BI$$

[4] R. J. Stirton, Test Department Technical Note 3038-55, January 1964, limited distribution.

The functional dependence $\Delta_j(I)$ is obtained experimentally. Figure 18 shows a typical response. It should be noted a linear system is required. The output pulse amplitude $S_{4,0}$ vs. I is shown in Fig. 19. This response is also linear.

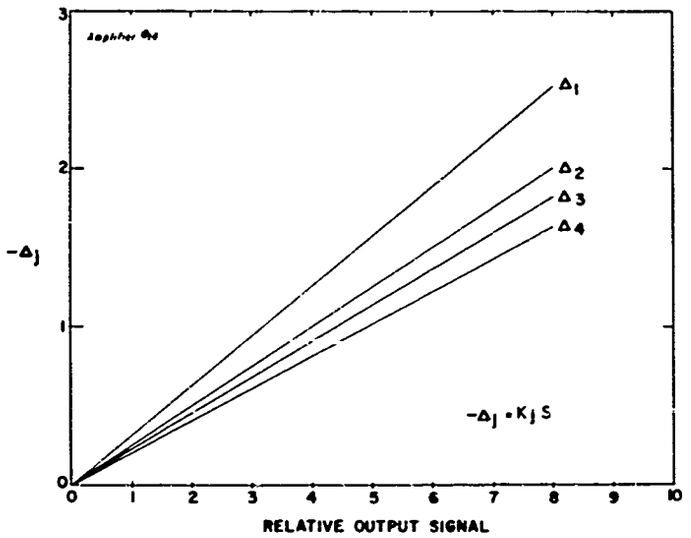

FIG. 18. Overshoot Compensation Parameters vs. Signal Level.

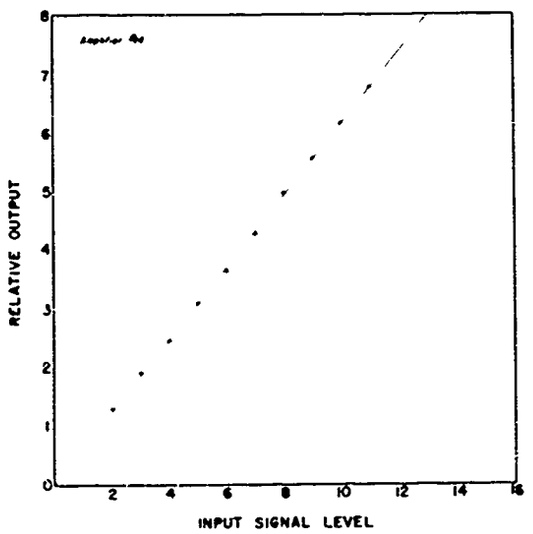

FIG. 19. Signal Amplifier Linearity.

The compensation functions can be written as

$$\Delta_j(I_i) = K_j I_i$$

where the value of K_j is determined from a calibration, and the full set of equations becomes:

$$S_{0,0} = BI_0 - K_1 I_4 - K_2 I_3 - K_3 I_2 - K_4 I_1$$

$$S_{1,0} = BI_1 - K_1 I_0 - K_2 I_4 - K_3 I_3 - K_4 I_2$$

$$S_{2,0} = BI_2 - K_1 I_1 - K_2 I_0 - K_3 I_4 - K_4 I_3$$

$$S_{3,0} = BI_3 - K_1 I_2 - K_2 I_1 - K_3 I_0 - K_4 I_4$$

$$S_{4,0} = BI_4 - K_1 I_3 - K_2 I_2 - K_3 I_1 - K_4 I_0$$

In the present application $I_0 = 0$ and when rearranged the set reduces to the nonhomogeneous set of linear equations:

$$K_4 I_1 + K_3 I_2 + K_2 I_3 + K_1 I_4 = -S_{0,0}$$

$$-BI_1 + K_4 I_2 + K_3 I_3 + K_2 I_4 = -S_{1,0}$$

$$K_1 I_1 - BI_2 + K_4 I_3 + K_3 I_4 = -S_{2,0}$$

$$K_2 I_1 + K_1 I_2 - BI_3 + K_4 I_4 = -S_{3,0}$$

$$K_3 I_1 + K_2 I_2 + K_1 I_3 - BI_4 = -S_{4,0}$$

where the first equation can be considered redundant. For simplicity, it is assumed that $B = 1$. In matrix form,

$$KI = -S_0$$

where

$$K = \begin{bmatrix} -1 & K_4 & K_3 & K_2 \\ K_1 & -1 & K_4 & K_3 \\ K_2 & K_1 & -1 & K_4 \\ K_3 & K_2 & K_1 & -1 \end{bmatrix}, \quad I = \begin{bmatrix} I_1 \\ I_2 \\ I_3 \\ I_4 \end{bmatrix}, \quad -S_0 = \begin{bmatrix} S_{1,0} \\ S_{2,0} \\ S_{3,0} \\ S_{4,0} \end{bmatrix}$$

To apply the compensation to general steady-state data, the following is required:

$$I = K^{-1} S_0$$

This compensation analysis is quite general with the limitation that the system be linear. Any number of pulses per frame is allowable although for practical purposes, inversion of matrices greater than 7 x 7 becomes prohibitive.

As a simple example of the use of this method, consider a direct-coupled system with fast response. In this case K_i = constant for all i and for the ROCOZ system with four samples and a zero measurement per frame, $K_i = 1/4$. A particularly simple result is obtained:

$$S_i = \frac{4}{21}\left(6\, S_{i,0} - \sum_{j=1}^{4} S_{j,0}\right), \quad j \neq i$$

For the ROCOZ photometer, it has been impossible to define a unique set of K_i's because of variability in the photocells and amplifiers and consequently individual calibrations are required.

REFERENCES

1. Inn, Edward C. Y., and Yoshio Tanaka. "Ozone Absorption Coefficients in the Visible and Ultraviolet Regions," in Ozone Chemistry and Technology. Washington, D. C., American Chemical Society, 1959. Advances in Chemistry Series #21, pp. 263-68.

2. Paetzold, H. K. "Messungen des atmosphärischen ozons," in Handbuch der Aerologie, ed. by W. Hesse. Leipzig, Akademische Verlagsgesellschaft, 1961. Pp. 458-531.

3. Vassy, Arlette. "Radio-sonde spéciale pour la mesure de la répartition verticale de l'ozone atmosphérique," J SCI METEOROL, Vol. 10, No. 38 (April/June 1958), pp. 63-75.

4. Kobayashi, J., M. Kyozuka, and H. Muramatsu. "On Various Methods of Measuring the Vertical Distribution of Atmospheric Ozone(I)," PAPERS METEOROL GEOPHYS (TOKYO), Vol. XVII, No. 2 (November 1966), pp. 76-96.

5. Chapman, S. "The Absorption and Dissociative or Ionizing Effect of Monochromatic Radiation in an Atmosphere on a Rotating Earth. Part I," PHYS SOC, PROC, Vol. 43 (1931), pp. 26-45.

6. Vigroux, E. "Contribution a l'étude expérimentale de l'absorption de l'ozone," ANN PHYS, Vol. 8 (1953), pp. 709-62.

7. Johnson, F. S., J. D. Purcell, R. Tousey, and K. Watanabe. "Direct Measurement of the Vertical Distribution of Atmospheric Ozone to 70 Kilometers Altitude," J GEOPHYS RES, Vol. 57 (1952), pp. 157-76.

8. Craig, Richard A. The Upper Atmosphere--Meteorology and Physics. New York, Academic Press, 1965.

UNCLASSIFIED
Security Classification

DOCUMENT CONTROL DATA - R&D

(Security classification of title, body of abstract and indexing annotation must be entered when the overall report is classified)

1 ORIGINATING ACTIVITY (Corporate author)

Naval Weapons Center
China Lake, California 93555

2a REPORT SECURITY CLASSIFICATION

UNCLASSIFIED

2b GROUP

3 REPORT TITLE

ROCKET OZONESONDE (ROCOZ)--DESIGN AND DEVELOPMENT

4 DESCRIPTIVE NOTES (Type of report and inclusive dates)

Research Report

5 AUTHOR(S) (Last name, first name, initial)

Krueger, A. J.; McBride, W. R.

6 REPORT DATE	7a TOTAL NO OF PAGES	7b NO OF REFS
July 1968	40	8

8a CONTRACT OR GRANT NO	9a ORIGINATOR'S REPORT NUMBER(S)
b PROJECT NO ONR 082-183	NWC TP 4512
c PMR PO-3-0021/072831005 PMR PO-4-0005/073146202	9b OTHER REPORT NO(S) (Any other numbers that may be assigned this report)
d	

10 AVAILABILITY/LIMITATION NOTICES

THIS DOCUMENT IS SUBJECT TO SPECIAL EXPORT CONTROLS AND EACH TRANSMITTAL TO FOREIGN GOVERNMENTS OR FOREIGN NATIONALS MAY BE MADE ONLY WITH PRIOR APPROVAL OF THE NAVAL WEAPONS CENTER.

11 SUPPLEMENTARY NOTES	12 SPONSORING MILITARY ACTIVITY
	Naval Air Systems Command Naval Material Command Washington, D. C. 20360

13 ABSTRACT

This report describes the theory and design of an optical ozonesonde system developed for use on Arcas rockets. The payload is an ultraviolet filter photometer useful in the altitude range 20 to 60 km. A real-time digital data logging system has been constructed for recording the data that are telemetered on the 1680 mHz meteorological frequency. Data-processing procedures are described and results of a test flight are presenced.

DD FORM 1473 (1 JAN 64) S/N 0101-807-6801

UNCLASSIFIED
Security Classification

14 KEY WORDS	LINK A		LINK B		LINK C	
	ROLE	WT	ROLE	WT	ROLE	WT
Rocket ozonesonde **Ozone distribution** **Arcas rocket** **Ultraviolet measurements** **Stratosphere**						

INSTRUCTIONS

1. ORIGINATING ACTIVITY: Enter the name and address of the contractor, subcontractor, grantee, Department of Defense activity or other organization *(corporate author)* issuing the report.

2*a*. REPORT SECURITY CLASSIFICATION: Enter the overall security classification of the report. Indicate whether "Restricted Data" is included. Marking is to be in accordance with appropriate security regulations.

2*b*. GROUP: Automatic downgrading is specified in DoD Directive 5200.10 and Armed Forces Industrial Manual. Enter the group number. Also, when applicable, show that optional markings have been used for Group 3 and Group 4 as authorized.

3. REPORT TITLE: Enter the complete report title in all capital letters. Titles in all cases should be unclassified. If a meaningful title cannot be selected without classification, show title classification in all capitals in parenthesis immediately following the title.

4. DESCRIPTIVE NOTES: If appropriate, enter the type of report, e.g., interim, progress, summary, annual, or final. Give the inclusive dates when a specific reporting period is covered.

5. AUTHOR(S): Enter the name(s) of author(s) as shown on or in the report. Enter last name, first name, middle initial. If military, show rank and branch of service. The name of the principal author is an absolute minimum requirement.

6. REPORT DATE: Enter the date of the report as day, month, year; or month, year. If more than one date appears on the report, use date of publication.

7*a*. TOTAL NUMBER OF PAGES: The total page count should follow normal pagination procedures, i.e., enter the number of pages containing information.

7*b*. NUMBER OF REFERENCES: Enter the total number of references cited in the report.

8*a*. CONTRACT OR GRANT NUMBER: If appropriate, enter the applicable number of the contract or grant under which the report was written.

8*b*, 8*c*, & 8*d*. PROJECT NUMBER: Enter the appropriate military department identification, such as project number, subproject number, system numbers, task number, etc.

9*a*. ORIGINATOR'S REPORT NUMBER(S): Enter the official report number by which the document will be identified and controlled by the originating activity. This number must be unique to this report.

9*b*. OTHER REPORT NUMBER(S): If the report has been assigned any other report numbers *(either by the originator or by the sponsor)*, also enter this number(s).

10. AVAILABILITY/LIMITATION NOTICES: Enter any limitations on further dissemination of the report, other than those imposed by security classification, using standard statements such as:

(1) "Qualified requesters may obtain copies of this report from DDC."

(2) "Foreign announcement and dissemination of this report by DDC is not authorized."

(3) "U. S. Government agencies may obtain copies of this report directly from DDC. Other qualified DDC users shall request through _____."

(4) "U. S. military agencies may obtain copies of this report directly from DDC. Other qualified users shall request through _____."

(5) "All distribution of this report is controlled. Qualified DDC users shall request through _____."

If the report has been furnished to the Office of Technical Services, Department of Commerce, for sale to the public, indicate this fact and enter the price, if known.

11. SUPPLEMENTARY NOTES: Use for additional explanatory notes.

12. SPONSORING MILITARY ACTIVITY: Enter the name of the departmental project office or laboratory sponsoring *(paying for)* the research and development. Include address.

13. ABSTRACT: Enter an abstract giving a brief and factual summary of the document indicative of the report, even though it may also appear elsewhere in the body of the technical report. If additional space is required, a continuation sheet shall be attached.

It is highly desirable that the abstract of classified reports be unclassified. Each paragraph of the abstract shall end with an indication of the military security classification of the information in the paragraph, represented as *(TS)*, *(S)*, *(C)*, or *(U)*.

There is no limitation on the length of the abstract. However, the suggested length is from 150 to 225 words.

14. KEY WORDS: Key words are technically meaningful terms or short phrases that characterize a report and may be used as index entries for cataloging the report. Key words must be selected so that no security classification is required. Identifiers, such as equipment model designation, trade name, military project code name, geographic location, may be used as key words but will be followed by an indication of technical context. The assignment of links, roles, and weights is optional.